Observation of a Kelvin-Helmholtz Instability in a High-Energy-Density Plasma on the Omega Laser

E. C. Harding,[1] J. F. Hansen,[2] O. A. Hurricane,[2] R. P. Drake,[1] H. F. Robey,[2] C. C. Kuranz,[1] B. A. Remington,[2] M. J. Bono,[2] M. J. Grosskopf,[1] and R. S. Gillespie[1]

[1]*University of Michigan, Ann Arbor, Michigan 48109, USA*
[2]*Lawrence Livermore National Laboratory, Livermore, California 94550, USA*

(Received 5 December 2008; published 24 July 2009)

A laser initiated experiment is described in which an unstable plasma shear layer is produced by driving a blast wave along a plastic surface with sinusoidal perturbations. In response to the vorticity deposited and the shear flow established by the blast wave, the interface rolls up into large vortices characteristic of the Kelvin-Helmholtz instability. The experiment used x-ray radiography to capture the first well-resolved images of Kelvin-Helmholtz vortices in a high-energy-density plasma.

DOI: 10.1103/PhysRevLett.103.045005 PACS numbers: 52.35.Tc, 47.20.Ft, 52.38.−r

The physical processes governing the evolution of a stratified fluid flow with a large velocity gradient (i.e., a shear flow) are of fundamental interest to a wide range of research areas including combustion, inertial confinement fusion (ICF), stellar supernovae, and geophysical fluid dynamics [1–5]. Traditional experiments have used inclined tanks of fluid to initiate a flow, generally at low Reynolds numbers, or wind tunnels that combine two parallel gas flows at the end of a thin wedge, known as a splitter plate. The splitter plate experiments have explored flows with maximum shear velocities on the order of 10^3 m/s and Reynolds numbers up to 10^6 [6,7]. Here we report the creation of a novel type of shear flow, achieved by confining a laser-driven blast wave in a millimeter-sized shock tube, which produced shear velocities on the order of 10^4 m/s and Reynolds numbers of 10^6 in a plasma.

These experiments are the first to observe the growth of perturbations by the Kelvin- Helmholtz (KH) instability under high-energy-density (HED) conditions. In most flows containing shear layers having steep enough velocity gradients, small perturbations that initially develop on an interface are amplified by KH, driven by lift forces that result from differential flow across the perturbation. HED plasmas are created when an energy source, a multikilojoule laser in this case, produces a plasma with a pressure of order one Mbar or more. Such plasmas are compressible, actively ionizing, often involve strong shock waves, and have complex material properties. The one previous attempt to produce a shear flow under HED conditions was inconclusive and did not observe KH growth [8].

The KH instability and shear flow effects in general are also of practical importance in a number of HED systems. They should be considered in multishock implosion schemes for direct drive capsules for ICF, since the KH instability may accelerate the growth of a turbulent mixing layer at the interface between the ablator and solid deuterium-tritium nuclear fuel [9,10]. Some approaches to ICF (e.g., fast ignition [11]) produce shear flows qualitatively similar to those discussed here. Some supernova explosion models also find that KH plays an important role [12,13]. In addition, the experiments and simulations of HED and astrophysical systems have shown that structures driven by shear flow appear on the high-density spikes produced by the Rayleigh-Taylor and Richtmyer-Meshkov instabilities [12,14]. Both Rayleigh-Taylor and Richtmyer-Meshkov have important consequences for the evolution of ionized, compressible flows, including those found in ICF [15] and astrophysical systems.

The present experiments (see Fig. 1) used rectangular, beryllium shock tubes, 4.0 mm long, with an interior width of 1.0 mm and height of 2.0 mm, 0.2 mm thick on the vertical walls and 0.5 mm thick on the horizontal walls. Two blocks of material each 1 mm tall were stacked within each shock tube. The upper block was carbonized-resorcinol-formaldehyde (CRF) foam ($C_{1000}O_{48}H_{65}$, density $\rho = 0.100$ g/cm^3 and average cell size 0.02 μm). The lower block was composed of three smaller pieces, glued together. The outer two pieces were polyamide-imide plastic ($C_{22}H_{14}O_4N_2$, $\rho = 1.42$ g/cm^3, referred to as PAI), each 0.40 mm wide. The smaller, center piece was 0.20 mm wide and was made of 3% iodinated polystyrene ($C_{50}H_{47}I_3$, $\rho = 1.45$ g/cm^3, referred to as CHI). Identical sinusoidal perturbations of wavelength $\lambda = 400$ μm and peak-to-valley amplitude $= 60$ μm were machined into one of the long faces of the CRF and PAI-CHI blocks, which were then mated along the perturbed side. One end of the shock tube and blocks was covered with a 30 μm thick polystyrene (C_8H_8, $\rho = 1.05$ g/cm^3) ablator. On top of the ablator was a 50 μm thick Au washer of outer diameter 2.5 mm, with an interior, square (1.0×1.0 mm) cutout that was aligned with the center of the CRF block. Attached to the shock tube was a shield that prevented the detection of radiation emitted from the laser-ablated plasma. Hurricane [16] describes the design of the shock tube components of this target.

The experiments were performed at the Omega laser facility at the Laboratory for Laser Energetics, University of Rochester [17]. The laser (Nd glass, $\lambda = 0.351$ μm)

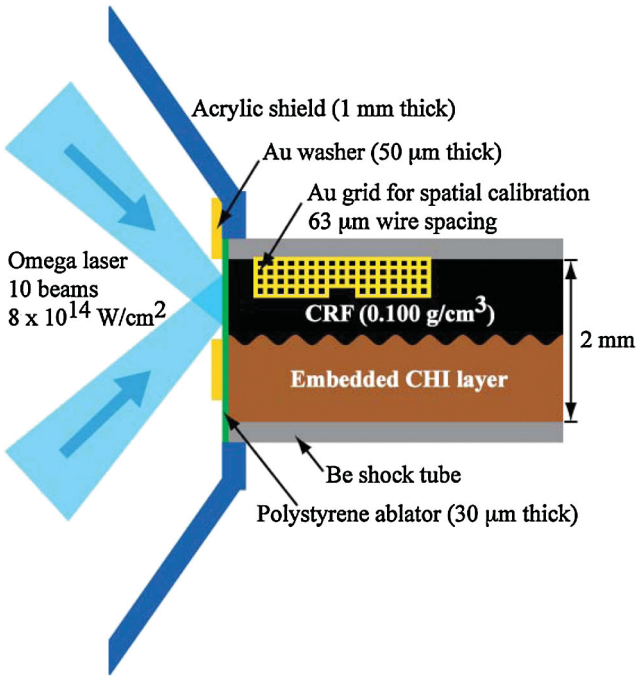

FIG. 1 (color). A cross-sectional view of the Kelvin-Helmholtz target. The sinusoidal perturbation had a wavelength of 400 μm and a peak-to-valley amplitude of 60 μm. The Au grid was attached to the outside of the shock tube, but it is shown here for clarity.

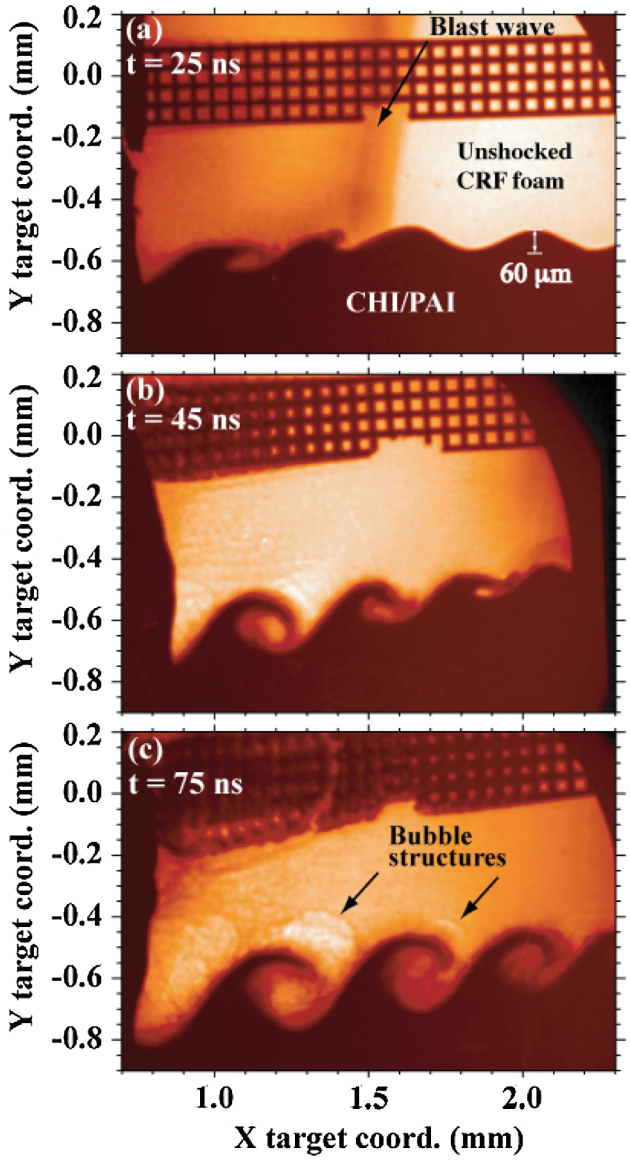

FIG. 2 (color). X-ray radiographs of three identical targets that show the formation of large Kelvin-Helmholtz roll-ups. These radiographs were captured at 25 ns (a), 45 ns (b), and 75 ns (c) after the start of the drive beam pulse. Here the origin of the x and y axes was defined by the nominal position of the drive beams on the polystyrene ablator. The placement of the axes on the images is accurate to within 10%. The Au grid was distorted by the blast wave when it broke out from the inside of the shock tube and struck the grid. These images are displayed with no postprocessing.

delivered 4.3 ± 0.1 kJ to the target by overlapping ten "drive beams" onto the ablator, centered in the square cutout of the gold washer. Each beam had a temporal profile with 100 ps rise and fall times, a nominally flat top, and a full width at half maximum of 1.0 ns, and had an intensity profile whose shape is described by $\exp[-(r/430\ \mu\text{m})^{4.7}]$, where r is the distance from the center of the profile. The peak intensity of all ten overlapped beams was 8×10^{14} W/cm^2. The low intensity wings of the laser spot were masked by the Au washer, which prevented the disruption of the PAI-CHI blocks and the surrounding Be shock tube.

X-ray radiography was used to diagnose the target evolution at $t = 25$, 45, and 75 ns with respect to the start of the drive beam pulse. At the specified time interval an additional three beams, each with a nominal energy of 450 J, a 1 mm diameter spot size, and a temporal pulse shape like that of the drive beams, were overlapped onto the rear of a $200 \times 200 \times 5$ μm V foil attached to a 2×2 mm polystyrene substrate. The laser-heated V plasma generated x rays from the He-α transition (5.18 keV). Some x rays propagated through the V foil and through a tapered (20 to 35 μm diameter) pinhole aperture in a 50 μm thick Ta substrate located 500 μm from the V foil and 10 mm from the center of the shock tube. The V x rays transmitted through the target were incident on a single piece Agfa D7 film, later digitized. The film was exposed for the temporal duration of the x-ray emission ($\sim$1 ns). The inherent spatial resolution of the image corresponds to the resolution element established by the pinhole size. Nearly all of the of the opacity of the target was concentrated in the CHI layer in the center of the shock tube.

The laser ablation of material from the polystyrene surface created an initially large pressure ($\sim$50 Mbar) that drove a strong shock into the polystyrene. When the

laser drive ended, a rarefaction wave was launched from the ablation surface and propagated to the shock front, which subsequently developed into a decelerating blast wave. The blast wave compressed, heated, and imparted forward momentum to the CRF foam, which led to the high-speed flow of ionized CRF plasma. At the CRF-CHI interface the blast wave was refracted into the CHI where it continued to propagate as a transmitted shock, in a direction nearly orthogonal to the blast wave. It was thus unable to impart significant forward velocity to the CHI. Consequently, a velocity gradient developed and vorticity was deposited at the interface.

A time sequence of three radiographs in Fig. 2 shows the development of vortices that were initiated from the sinusoidal perturbations, and later driven to large amplitudes by the flow of CRF plasma that was created by the blast wave. Immediately after the blast wave passed, the crest of a perturbation mass appeared to be stripped in a process perhaps similar to that described by Hansen *et al.* [18]. Reflected shock waves that further increase the local density are seen emanating from the perturbation behind the blast wave in Fig. 2(a) and the rightmost perturbation in Fig. 2(b). In Fig. 2(c) the structure seen in the cores appeared to dissolve in the most developed roll-up, which may indicate the beginning of a transition to turbulence.

Measurements of the blast wave position in Fig. 2(a) indicate that it had traveled ~1500 μm in the first 25 ns, with an average speed of 60 ± 8 μm/ns. As the blast wave satisfies the requirements for self-similar behavior, its time-dependent position $\chi(t)$ can be modeled as a one-dimensional self-similar, planar blast wave, having $\chi(t) = At^{\alpha}$ where $\alpha = 3/5$ for a polytropic gas with $\gamma = 1.4$ [19]. The constant A was determined by the position of the blast wave in Fig. 2(a) and is equal to 220 ± 30 μm/ns$^{3/5}$. Using this equation we can estimate the time at which the blast wave passed each of the perturbations. Figure 3 shows the height of the perturbation as a function of the time elapsed since the leading edge of the blast wave was centered on the crest of a perturbation. Thus, the first four points are from Fig. 2(a), while the next six points are from the three leftmost roll-ups in Figs. 2(b) and 2(c). The x-ray attenuation measured from the data of Fig. 2(a) implies a maximum shocked foam density of 0.39 ± 0.04 g/cm^3. However, this simple measurement assumed that the blast wave was parallel to the diagnostic line of sight (0° tilt), and did not account for the finite resolution of the diagnostic or the blurring due to the motion of the blast wave. By including all of these effects in a three-dimensional model of the blast wave, the observed data was fit well by a modified self-similar density profile that had a maximum density of 0.9 g/cm^3 ($\gamma = 1.25$) and a 9° tilt. The tilting of the blast wave was primarily responsible for the apparent broadening of the intensity distribution of the blast wave seen in Fig. 2(a). Strong shock conditions were assumed with a nominal $\gamma = 1.4$ for the following calculations of the post-shock-flow speed, pressure, foam temperature (T_s), average ionization state (Z), and kinematic viscosity (ν). The uncertainties given include the variations of these quantities that result from using $\gamma = 1.25$. By requiring the conservation of mass flux and energy density across the blast wave, we find that foam plasma immediately behind the blast wave had a speed of 50 ± 7 μm/ns and a pressure of 3 ± 1 Mbar. Assuming electron-ion equilibrium, T_s can be estimated by $2(\gamma - 1)Am_p u_s^2/[(1 + Z)(\gamma + 1)^2]$ where γ is the adiabatic index of the shocked foam, A is the atomic mass of the foam, m_p is the proton mass, and u_s is the blast wave speed [20]. Analytical fits to the Thomas-Fermi ionization model [21] were used to iteratively solve for Z until it was consistent with the above equation for T_s. This process yields $T_s = 18 \pm 7$ eV and $Z = 2.4 \pm 0.4$. Inserting these values into a known equation for kinematic viscosity [22] gives $\nu = 0.014 \pm 0.007$ cm^2/s, which leads to an initial Reynolds number of 10^6 using a post-shock velocity of 50 μm/ns and a scale length of 60 μm.

In Fig. 3 a discrete vortex model with a constant circulation $\Gamma = 4700$ μm^2/ns was used to calculate the time-dependent growth of the perturbations, starting from a compressed height of 44 μm [16,23]. In the experiment the roll-ups are further stretched by the decompression of the shocked CHI, which is not now included in the model and perhaps why the model underestimates the height of the roll-up later in time. Figure 3 shows the incompressible KH growth rate from the linearized fluid equations [24] for constant shear velocities (ΔU) of 50 μm/ns and 12 μm/ns, which was the average velocity calculated

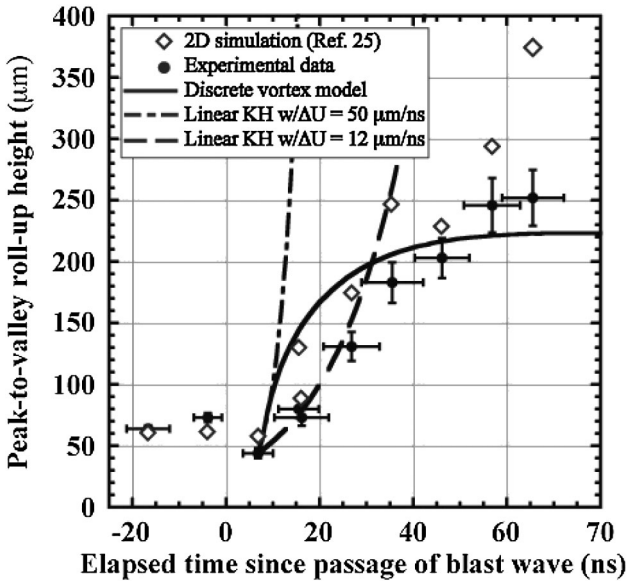

FIG. 3. Experimental measurements of the peak-to-valley KH roll-up heights (observed over multiple targets) compared with several analytical models. All models assume the growth starts from the measured compressed perturbation height of 44 μm.

from the self-similar velocity profile over the ~30 ns time period it takes the velocity to decay to zero.

Simulations of this experiment face their own challenges. These include the uncertainty in the equation of state of the foam, laser absorption treatments that are not fully three dimensional, and the problem of the resolution of small-scale structures. Figure 3 also shows results from preliminary two-dimensional simulations, discussed elsewhere in [25], that overestimated the average blast wave velocity in the first 25 ns by ~20%. The time used for the simulation data points in Fig. 3 was the time elapsed when the simulated blast wave reached a given crest. Within their limitations, these simulations are in reasonable agreement with the data.

The source of bubblelike structures that appear to emanate from the downstream side of the leftmost roll-up in Fig. 2(b) and the two-leftmost roll-ups in Fig. 2(c) is not known. Similar bubble structures have not been observed in any previous HED experiment. Based on the observed x-ray attenuation, the densities associated with these structures are as follows. The brighter regions within the largest bubble in Fig. 2(c) had densities of $0.03(+0.06, -0.03)$ g/cm^3, while those of the dark rim of the bubble were 0.21 ± 0.06 g/cm^3. Uniform regions outside the bubble had densities of 0.10 ± 0.06 g/cm^3. The measured average density difference between the exterior and interior of bubble ($\rho_{\text{out}} - \rho_{\text{in}}$) was 0.09 ± 0.03 g/cm^3. The bubbles appeared to be expanding at ~10 μm/ns. Reference [25] shows that the bubbles are not now reproduced by two-dimensional simulations, and offers several hypotheses concerning their origins. The current uncertainty in the equation of state of the CRF foam is certainly a major limitation. We speculate that the formation of the bubbles may be associated with the velocity reversal of the CRF flow. The bubbles may also have some connection with the ''shocklets'' discussed as a theoretical possibility by Dimotakis [26].

In conclusion, this experiment is significant because it demonstrates a novel method for creating a shear flow and is the first to create a diagnosable KH instability in a HED system. Understanding the KH instability is important because it plays a central role in the transition to turbulence in many HED, astrophysical, and other fluid systems. We observed unique bubblelike structures whose origins are still under investigation. Currently, simulations are unable to reproduce these bubbles, indicating that this shear flow experiment provides a rigorous test for benchmarking numerical simulations. Future laser-driven experiments, using steady shocks rather than blast waves, could create a more sustained flow with a higher Reynolds number in order to drive the system to a fully turbulent state.

The authors acknowledge Chuck Sorce, Omega Operations Staff, LLNL Target Fabrication, and Michigan Target Fabrication for their outstanding support. This research was sponsored by the Stockpile Stewardship Academic Alliances program through DOE Research Grant No. DE-FG52-07NA28058, and by DOE Research Grant No. DE-FG52-04NA00064 and other grants and contracts.

[1] S. A. Thorpe, J. Geophys. Res. **92**, 5231 (1987).
[2] E. Gutmark *et al.*, Combust. Sci. Technol. **66**, 107 (1989).
[3] M. H. Emery, J. H. Gardner, and J. P. Boris, Phys. Rev. Lett. **48**, 677 (1982).
[4] R. A. Chevalier, J. M. Blondin, and R. T. Emmering, Astrophys. J. **392**, 118 (1992).
[5] C. C. Wu, J. Geophys. Res. **91**, 3042 (1986).
[6] D. Papamoschou and A. Roshko, J. Fluid Mech. **197**, 453 (1988).
[7] G. L. Brown and A. Roshko, J. Fluid Mech. **64**, 775 (1974).
[8] B. A. Hammel *et al.*, Phys. Plasmas **1**, 1662 (1994).
[9] K. O. Mikaelian, Phys. Fluids **6**, 1943 (1994).
[10] P. Diamond *et al.*, in JASON Report No. JSR-91-325, MITRE Corporation, 1993.
[11] M. Roth *et al.*, Phys. Rev. Lett. **86**, 436 (2001).
[12] K. Kifonidis *et al.*, Astron. Astrophys. **408**, 621 (2003).
[13] J. C. Wheeler, J. R. Maund, and S. M. Couch, Astrophys. J. **677**, 1091 (2008).
[14] A. R. Miles *et al.*, Phys. Plasmas **11**, 3631 (2004).
[15] S. Atzeni and J. Meyer-ter-Vehn, *The Physics of Inertial Fusion : Beam Plasma Interaction, Hydrodynamics, Hot Dense Matter* (Oxford University Press, Oxford, 2004).
[16] O. A. Hurricane, High Energy Density Phys. **4**, 97 (2008).
[17] T. R. Boehly *et al.*, Opt. Commun. **133**, 495 (1997).
[18] J. F. Hansen *et al.*, Phys. Plasmas **14**, 056 505 (2007).
[19] I. B. Zeldovich and I. P. Raizer, *Physics of Shock Waves and High-Temperature Hydro* (Academic Press, New York, 1966).
[20] R. P. Drake, *High-Energy-Density Physics: Fundamentals, Inertial Fusion and Experimental Astrophysics* (Springer, New York, 2006).
[21] D. Salzmann, *Atomic Physics in Hot Plasmas* (Oxford University Press, New York, 1998).
[22] J. G. Clerouin, M. H. Cherfi, and G. Zerah, Europhys. Lett. **42**, 37 (1998).
[23] A. Rikanati, U. Alon, and D. Shvarts, Phys. Fluids **15**, 3776 (2003).
[24] S. Chandrasekhar, *Hydrodynamic and Hydromagnetic Stability* (Dover, New York, 1961).
[25] O. A. Hurricane *et al.*, Phys. Plasmas **16**, 056305 (2009).
[26] P. E. Dimotakis, in *Progress in Astronautics and Aeronautics*, edited by S. N. B. Murthy and E. T. Curran (AIAA, Washington, DC, 1991), p. 265.